**Proceedings of the ASME 2013 International Design Engineering Technical Conferences &
International Conference on Advanced Vehicle Technologies
IDETC/AVT 2013
August 4-7, 2013, Portland, USA**

DETC2013-13486

EXPERIMENTAL VALIDATION OF A VOLUMETRIC PLANETARY ROVER WHEEL/SOIL INTERACTION MODEL

Willem Petersen
Department of Systems Design Engineering
University of Waterloo
Waterloo, Ontario, N2L 3G1
Canada
Email: wpeterse@uwaterloo.ca

John McPhee
Department of Systems Design Engineering
University of Waterloo
Waterloo, Ontario, N2L 3G1
Canada
Email: mcphee@uwaterloo.ca

ABSTRACT

For the multibody simulation of planetary rover operations, a wheel-soil contact model is necessary to represent the forces and moments between the tire and the soft soil. A novel nonlinear contact modelling approach based on the properties of the hypervolume of interpenetration is validated in this paper. This normal contact force model is based on the Winkler foundation model with nonlinear spring properties. To fully define the proposed normal contact force model for this application, seven parameters are required. Besides the geometry parameters that can be easily measured, three soil parameters representing the hyperelastic and plastic properties of the soil have to be identified. Since it is very difficult to directly measure the latter set of soil parameters, they are identified by comparing computer simulations with experimental results of drawbar pull tests performed under different slip conditions on the Juno rover of the Canadian Space Agency (CSA). A multibody dynamics model of the Juno rover including the new wheel/soil interaction model was developed and simulated in MapleSim. To identify the wheel/soil contact model parameters, the cost function of the model residuals of the kinematic data is minimized. The volumetric contact model is then tested by using the identified contact model parameters in a forward dynamics simulation of the rover on an irregular 3-dimensional terrain and compared against experiments.

INTRODUCTION

In the past, robotic vehicles have been a very beneficial tool for a number of planetary exploration projects. Relatively recent projects include the Spirit and Opportunity rovers that were sent to Mars, in the most successful rover exploration missions as of today. For the simulation of these types of planetary rovers, a crucial component of the vehicle dynamics model is the wheel/soil interaction, which requires accurate prediction of the contact forces within a reasonable computation time. The biggest challenge for these types of contact models is to calculate the forces in the contact patch due to the large deformation of the soft soil. A number of rigid and flexible planetary rover wheel models were proposed by researchers [1–7] and they all use a certain soil pressure-sinkage equation to relate the distributed forces in the contact interface to the compression of the soil. The resultant contact force is then calculated by integration of said pressure-sinkage relation.

In this paper, a nonlinear wheel/soil contact model is proposed and validated using planetary rover experiments. This new approach is based on the volumetric properties of the contact problem providing a closed-form expression for the wheel forces [8, 9]. All of the commonly used soil pressure-sinkage relations can be applied to the proposed theory to represent the hyperelastic properties of the soil; however, the Bernstein-Goriatchkin relation is used in this paper to derive the equations for the nonlinear volumetric wheel/soil model. Furthermore, the plastic behaviour of soft soils has to be considered when calculating the

contact forces between the wheel and the terrain. A common representation of plasticity is the assumption that the soil does not relax after compression. This means that all of the energy that is needed to compact the soil dissipates. Even if most soils show very little relaxation, a small amount of recoil in the hyperelastic foundation springs can affect the forces predicted by the contact model. In this work, the plasticity is represented by the soil rebound, which is a nondimensional parameter dependent on the maximum sinkage of the wheel. Finally, the tangential planetary rover wheel forces are calculated using a friction-like model based on the volumetric normal forces and the Mohr-Coulomb criterion [9]. As a result, the proposed wheel/soil model utilizes the following four parameters to represent the hyperelastic soil foundation and soil plasticity.

1. k_h hyperelastic stiffness
2. η nonlinearity exponent
3. γ soil rebound
4. K_{v_x} traction modulus

Additionally, the remaining contact model parameters are all dependent on the assumed geometry of the wheel. While these wheel parameters can be easily measured, the soil parameters of wheel/soil contact models have to be determined through rigorous experiments such as Bekker's compression test with a Be-Vameter. In this work, a drawbar pull test is used to identify the model parameter values using experimental data from a prototype of the Juno rover of the CSA. An unconstrained nonlinear optimization routine is implemented to determine the soil parameters in an iterative manner. Furthermore, the proposed planetary rover wheel model is simulated on a 3-dimensional terrain using the found parameters. For validation purposes, the simulation results are compared against experiments of the CSA Juno rover on the same irregular terrain. This two-step validation process sufficiently verifies the adequacy of the proposed model.

This paper is an extension to previous work by the authors [10], which discusses the identification of normal pressure-sinkage relation parameters. In this work, the development of a fully volumetric planetary rover wheel requires the introduction of further parameters that are identified and validated through an extended set of rover experiments.

VOLUMETRIC WHEEL/SOIL INTERACTION MODEL

The highly nonlinear properties of soft soils are represented using a foundation of hyperelastic springs. The integration of the nonlinear stress distribution over the contact surface results in the following Eqn 1 for the normal force $\mathbf{F}_n$:

$$\mathbf{F}_n = k_h \int_S f_S^{\eta}(\mathbf{S})\, dS\, \mathbf{n} \tag{1}$$

By solving the integral of the hyperelastic spring displacements, it can be shown that the normal contact force is now proportional to an $(\eta+2)$-dimensional hypervolume with the hyperelastic foundation stiffness as the proportionality factor [8]. Eqn 1 can therefore be simplified to the following Eqn 2:

$$\mathbf{F}_n = k_h V_h\, \mathbf{n} \;\text{ with } V_h = \int_S f_S^{\eta}(\mathbf{S})\, dS \tag{2}$$

where V_h is the hypervolume of penetration. By introducing the definition of the hypervolume, the challenge is to solve the integral of Eqn 2. In fact, for most nonlinearity exponents η, an analytical solution does not exist even under the assumption of very basic contact geometries. To find an approximation for the integral, the hypervolume model is assumed to be a function of the penetration volume and an explicit normal force expression can be derived [8, 9]. In this paper, the following equation is used to calculate the normal force between a perfect cylinder in contact with a locally even ground:

$$\mathbf{F}_n = k_h \left(\frac{V}{V_{int}}\right)^{A_1(\eta-1)} V\, \mathbf{n} \tag{3}$$

where the parameters A_1 and V_{int} are related to the contacting geometries and can be calculated through simple numerical experiments [8].

To fully define the tire forces, the tangential forces also have to be calculated. The longitudinal force that defines the tractive effort of a vehicle is limited by the shear bearing capabilities of the soil. The tangential forces in the soil and tire interface can be calculated by integrating the shear stress over the contact area [2]. However, to entirely utilize the computational advantage of the volumetric approach to model the contact between a rigid planetary rover wheel and the soft soil, the calculation of tangential contact force should be simplified to an explicit expression. Usually determined by integrating the shear stress as a function of the normal stress distribution and the shear displacement over the contact patch, this classical terramechanics approach shows limits for certain contact conditions [11]. In fact, for large contact patches and/or under high slip conditions, the shear limit in the contact patch is rapidly reached and the resultant nearly constant shear stress leads to a tangential force model with the longitudinal velocity and slip as its main influential factors. With that in mind and inspired by tire models commonly used in road vehicle dynamic simulations in which the traction force is a function of longitudinal velocity and slip, a fully volumetric soil shear force model can be achieved by assuming a friction-like model with an upper shear force limit as shown in Eqn 4.

$$F_t = F_{\tau_{max}} f\left(v_x, S_{long}\right) \tag{4}$$

where v_x and S_{long} are the longitudinal velocity component and the longitudinal slip respectively. $F_{\tau_{max}}$ is the shear force limit defined by the Mohr-Coulomb envelope and the function $f\left(v_x, S_{long}\right)$ has to be determined through experimental results. In fact, if single wheel test bed measurements are available, this type of model definition seems more intuitive than curve-fitting the shear stress as a function of the shear displacement. However, the resultant curve-fit requires the use of parameters that are related to the contact pairing rather than to the soil only. For most planetary rover operations, the model can be further simplified with longitudinal slip as the only kinematic dependency variable. Hence, the proposed volumetric tangential force model as a hyperbolic function of longitudinal slip shown in Eqn 5 is based on typical single wheel test results [12].

$$F_t = F_{\tau_{max}} \tanh\left(\frac{S_{long}}{K_{v_x}}\right) \quad (5)$$
$$\text{with } F_{\tau_{max}} = AC + F_n \tan\phi$$

where A is the contact patch area, and C and ϕ are the soil parameters of cohesion and internal friction angle, respectively. The only curve-fit parameter used in this representation of the tangential force is the dimensionless shear velocity modulus K_{v_x}.

Before the developed contact model can be applied to planetary rover wheels in contact with soft soil, the plastic properties of the soil have to be addressed. Often, soil plasticity is modelled with springs that do not recoil but stay at a maximum compaction. This means that all energy that is used to compress the soil dissipates, which overestimates the compaction resistance and consequently influences the prediction of the wheel sinkage of such models. Even if most soils show very little relaxation, it influences the contact forces. In this model the dimensionless parameter of soil rebound γ is introduced to calculate the soil rebound as a linear function of the maximum sinkage. This model of the soil plasticity is applied to the contact geometry as shown in Figure 1. Assuming the illustrated contact geometry, the developed hypervolume model can be applied to calculate the normal force and with it the tangential contact force. The definition of the contact normal direction determines the contribution of these forces to the vertical and longitudinal tire force. In this model, the point of force application is defined by the centroid of the hypervolume of penetration, and the angle α as seen in Figure 1 defines the direction of the normal forces. The normal force can be calculated with Eqn 3 as presented earlier and the contact normal vector is determined using Eqn 6.

$$\mathbf{n} = -\frac{\mathbf{r}_{hc}}{|\mathbf{r}_{hc}|} \quad (6)$$
$$\text{with } \alpha = \arctan\frac{r_{hc,x}}{r_{hc,z}} \quad (7)$$

where $\mathbf{r}_{hc}$ is the position vector of the hypervolume centroid with respect to the wheel hub frame.

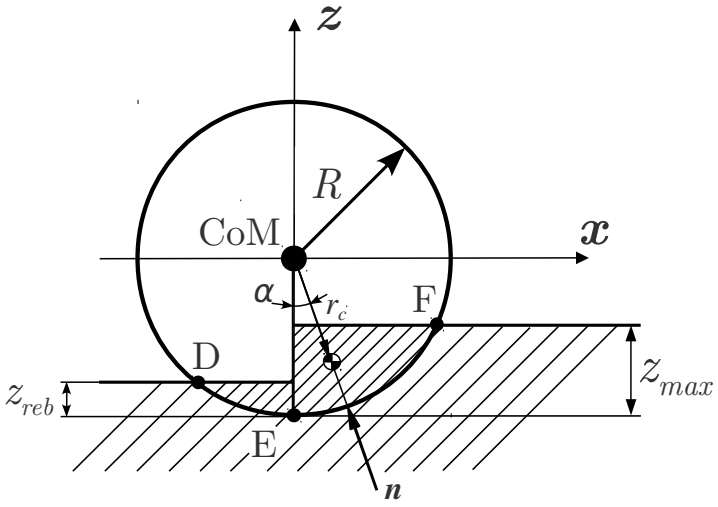

FIGURE 1. VOLUMETRIC WHEEL/SOIL MODEL SCHEMATIC

The normal force component in x-direction is the soil resistance due to compaction and the component of the normal force in z-direction represents the vertical tire force which supports the wheel load given by the weight and the dynamics of the rover. To determine the tire forces, the components of the normal force have to be summed up with the components of the tangential force. The x-component of the tangential force represents the traction force generated in the contact patch and the tangential force component in z-direction also supports the load of the wheel. This completes the hypervolumetric model of the tire forces which are now fully represented using the properties of the volume of interpenetration.

$$F_x = F_t \cos\alpha - F_n \sin\alpha \quad (8)$$
$$F_z = F_n \cos\alpha + F_t \sin\alpha \quad (9)$$
$$\text{with } F_n = k_h V_h$$

The developed tire model is then implemented into a model of the Juno rover from the Canadian Space Agency (CSA). This model is developed in the simulation software MapleSim including the volumetric wheel/soil interaction model and validated in a two step process. For this validation process, experimental data of the CSA Juno rover from two different experiments were collected: a drawbar pull test on flat terrain and rover run over 3-dimensional terrain. The first step in the validation process is to identify the unknown soil foundation parameters using the drawbar pull test. The second step is a forward dynamics simulation of the rover

on the 3-dimensional terrain to verify the identified parameters, and consequently the developed planetary rover wheel model, by comparing the results with the corresponding experimental data. The following sections describe the CSA Juno rover as well as the two-step validation process in detail.

JUNO ROVER

A prototype of the CSA Juno rover was used to collect the data of the two different experiments. A picture of the rover can be seen in Figure 2.

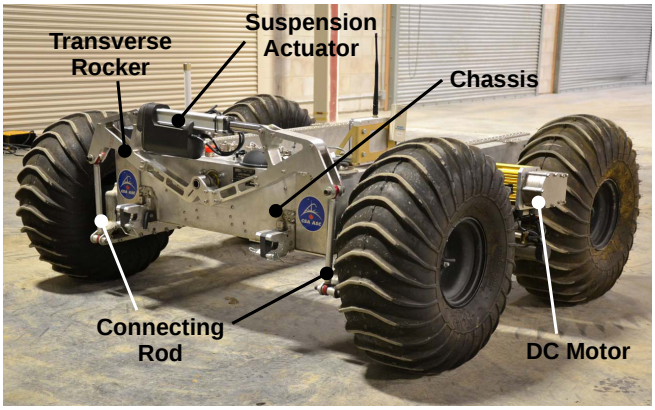

FIGURE 2. JUNO ROVER

The Juno rover is a skid-steered four wheel vehicle with dependent three rocker suspension. The two wheels on each side are connected to the main rockers and a transverse rocker attached to the rear end of the rover chassis constrains the movement of two main rockers through a connecting rod on each side. The configuration can be seen in the picture as it shows the rear of the rover. Two DC motors drive the rover, one attached to each of the main rocker. The wheels on each side are driven by a 1:1 chain wheel drive that is powered by the motor through a two gear transmission with gear ratios of 1:129 and 1:32 for the lower gear and the higher gear respectively. This way, each side can be driven individually, whereas the two wheels on each side are constrained to the same angular velocity. The total mass of the rover is 317.7 kg including the 22" wheels each of which weighs 9.6 kg. The wheels on the Juno prototype are lugged ARGO tires on a steel rim and it should be mentioned that the presented diameter of the wheels includes the dimensions of the tire tread or lugs on the tire. Although the Juno Rover design includes pneumatic tires, the assumption of rigid wheel is made based on the fact that the deformation of the terrain material is significantly larger than the deflection of the pneumatic tire. This soil deformation under the rover wheel creates a large contact patch over which the contact pressure in distributed. The result of such pressure distribution is a reduction of localized tire deformation and the effect of deformation parameter in the tire model is assumed to be negligible.

The rover is equipped with a number of sensors and measuring devices. In addition, a total station is used to track the global rover position via a prism that is attached to the rover. The recorded measurements for the presented experiments are the positions of the motor encoders, the current drawn by the motors, and the data from the inertia measurement unit (IMU). Furthermore, for the drawbar pull test and the irregular terrain experiment, a load cell was used to measure the drawbar pull and a LIDAR scanner was used to scan the 3-dimensional terrain surface respectively. The load cell was attached to the rear of the rover to record the applied resistive force, whereas the LIDAR scanner was used to scan the surface before and after each experiment.

IDENTIFICATION OF WHEEL/SOIL INTERACTION MODEL PARAMETERS

Besides the inertia and geometry parameters of the wheel, the implemented planetary rover wheel model includes the four soil foundation parameters $\mathbf{a} = [k_h, \eta, \gamma, K_{v_x}]$. While the inertia and geometry parameters can be easily measured, the listed soil parameters are difficult to obtain. To tune these parameters, a drawbar pull test is performed and the results are compared against the simulation results of the Juno rover obtained from a full vehicle model implemented in MapleSim. A figure of the developed rover model can be seen in Figure 3.

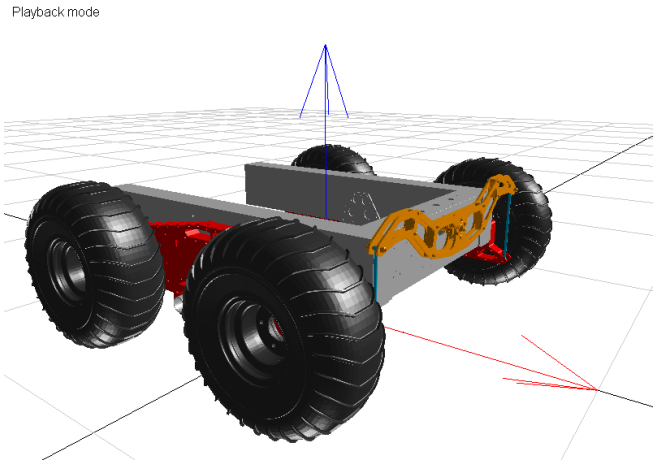

FIGURE 3. JUNO ROVER MODEL AS IMPLEMENTED IN MAPLESIM

By minimizing the difference between the experimental and

simulation results, an unconstrained optimization procedure is used to approach a set of realistic model parameters. All experiments were performed in a 15×7 $[m]$ sand box with an average depth of approximately 0.25 $[m]$. The terrain was prepared and loosened before each experiment. It was observed during the drawbar pull test that the terrain properties varied significantly over the prepared track; however, for simplicity, a homogeneous soil with averaged soil parameters was identified.

The drawbar pull force and the wheel drive torques are measured and applied as simulation inputs to the vehicle model, where matching the forward velocity and the wheel spin measurements define the optimization objective. The results of these measurements are included in a basic optimization routine and the missing parameters are identified through an iterative process by minimizing the residual of kinematic errors. The following cost function $\Omega(\mathbf{a})$ is defined. It consists of the sum of the weighted squared residuals of longitudinal velocity of the rover and the individual wheel spins assuming that $v_{x,i}$, $\omega_{y,i}$ are known at any measured instant of time t_i from the experiments.

$$\Omega(\mathbf{a}) = \sum_{i=1}^{n_{sim}} w_1 \, res_{v_x}(\mathbf{a})^2 + w_2 \, res_{\omega_y,right}(\mathbf{a})^2 + w_3 \, res_{\omega_y,left}(\mathbf{a})^2 \tag{10}$$

$$\text{with} \quad res_{v_x}(\mathbf{a}) = \frac{1}{R}\left(v_{x,i} - v_{x,sim}(t_i)\right) \tag{11}$$

$$res_{\omega_y,left}(\mathbf{a}) = \left[\omega_{y,i} - \omega_{y,sim}(t_i)\right]_{left} \tag{12}$$

$$res_{\omega_y,right}(\mathbf{a}) = \left[\omega_{y,i} - \omega_{y,sim}(t_i)\right]_{right} \tag{13}$$

where $res_{v_x}(\mathbf{a})$, $res_{\omega_y,right}(\mathbf{a})$, and $res_{\omega_y,left}(\mathbf{a})$ are the residuals of the forward speed, the wheel spins of the right side and the wheel spins of the left side, respectively, and w_1, w_2, and w_3 are the weights to these residuals, respectively. The summation limit n_{sim} is the number of time steps in the simulation performed in each iteration of the optimization. It should be noted that this number may vary from one iteration step to another. The residual res_{v_x} of the forward velocity is divided by the nominal wheel radius R so that the terms in the objective function are of the same units. The presented cost function defines the quadratic performance measure and the resulting least squares problem is solved using an unconstrained nonlinear optimization method based on the Nelder-Mead algorithm. The weights are chosen to eliminate numerical significance based on the numerical difference of the forward speed and the wheel spin, where the forward speed and the combined wheel spins from both sides are assumed to be of equal significance.

$$w_1 = \frac{\omega_{y,i}}{\frac{v_{x,i}}{R} + \omega_{y,i}}, \; w_2 = \frac{1}{2}\frac{\frac{v_{x,i}}{R}}{\frac{v_{x,i}}{R} + \omega_{y,i}}, \text{ and } w_2 = \frac{1}{2}\frac{\frac{v_{x,i}}{R}}{\frac{v_{x,i}}{R} + \omega_{y,i}}$$

It should be noted that the weights are different for each parameter identification procedure depending on the desired forward speed and wheel spin measured from the corresponding set of experimental results. The following sections explain the procedure and the results of the drawbar pull experiment, and discuss the identified parameters.

Drawbar Pull Experiments

For this particular experiment the rover is operated on flat and uncompacted soft soil. To achieve these conditions, the terrain within the test area was prepared before every run of the drawbar pull test. During each of these runs, the rover is forced to move at a constant speed through an applied force that provides enough resistance to provoke longitudinal slip. The rover is driven at a constant throttle setting and slowed down to a constant speed through a human-controlled resistive force applied to the rear end of the rover chassis. By controlling the applied drag force, the goal was to force the rover to settle at a constant slip condition. The rover may start outside the prepared terrain test area to allow for said settling process. In addition to the measurement equipment of the rover and the total station, a load cell was used to record the applied resistive force during each iteration of the experiment. The following list summarizes the crucial measurements that were taken during this experiment:

Rover IMU — chassis acceleration (three axis)
Motor — current measurement (left and right side)
Motor encoder — angular velocity (left and right side)
Total station — rover position (through prism attached to rover chassis)
Load cell — drawbar pull force

In total, three runs with individual data sets are considered and a parameter identification process for each of these data sets is conducted. The results of each drawbar pull test run as well as the corresponding optimization routines are explained in detail in the following sections. The resulting parameter sets are compared with each other.

First Drawbar Pull Experiment The first drawbar pull test was performed over a period of approximately $22s$ on an even and flat terrain. Due to difficulties in controlling the forward velocity of the rover to a constant speed with the applied force, the results of a period of $10s$ (starting at $8s$) were used, during which the rover had reached nearly steady-state conditions. Furthermore, due to the assumption of constant soil parameters, the average values of each measurement over this $10s$ period were taken and applied to the optimization routine. Figure 4 shows the measured drawbar pull force and drive torque that define the simulation inputs to the rover model.

The plots show the recorded drawbar pull force and the measured drive torque as well as the averaged values that are applied

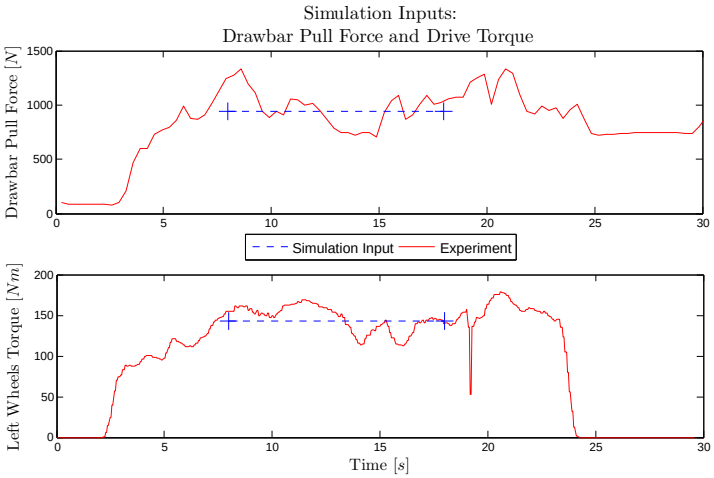

FIGURE 4. OPTIMIZATION INPUTS FROM EXPERIMENTAL DATA OF THE 1ST DRAWBAR PULL TEST

to the vehicle model. Considering these simulation inputs, the goal of the optimization is to reach the measured wheel spin and forward velocity of the rover by changing the parameters **a**. Figure 5 shows the measured longitudinal velocity and wheel spin that define the optimization objectives.

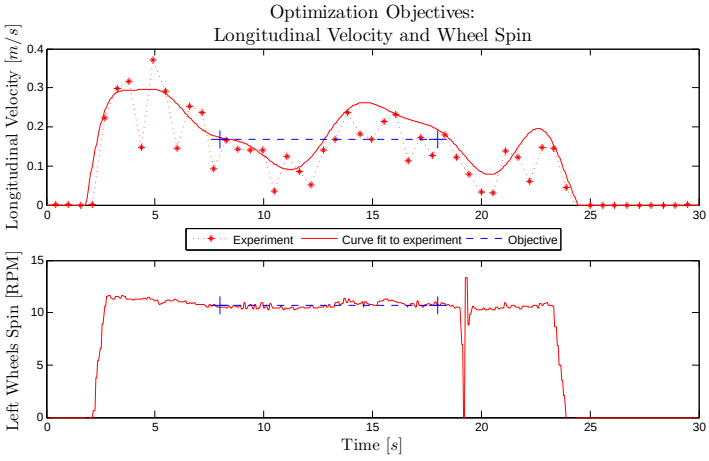

FIGURE 5. OPTIMIZATION OBJECTIVES FROM EXPERIMENTAL DATA OF THE 1ST DRAWBAR PULL TEST

The plots show the longitudinal velocity determined from the total station measurements and the wheel spin determined from the motor encoder recordings as well as the averaged values that are considered during the optimization routine. This concludes the required experimental data to identify the missing parameters using the cost function shown in Eqn 10. Table 1 shows the initial and final values of the soil parameters **a** for the first drawbar pull test.

TABLE 1. WHEEL AND SOIL MODEL PARAMETERS FOR 1ST DRAWBAR PULL EXPERIMENT

Model Parameter	Initial Value	Final Value
Foundation Stiffness k_h $[N/m^{2+\eta}]$	$2.5E10^5$	$2.07E0^5$
Nonlinearity Exponent η	0.5	0.583
Foundation Rebound γ [%]	0.15	0.0674
Traction Modulus K_{v_x}	0.5	0.689

The initial parameters were chosen based on the weight of the rover and an estimation of the required traction force. Once these parameters have been confirmed by the other drawbar pull experiments, they can be tested in a forward dynamic simulation of the rover on a 3-dimensional terrain.

Second Drawbar Pull Experiment The second run of the drawbar pull test was performed over a period of approximately 35s. Figure 6 shows the measured drawbar pull force and drive torque that define the simulation inputs to the rover model.

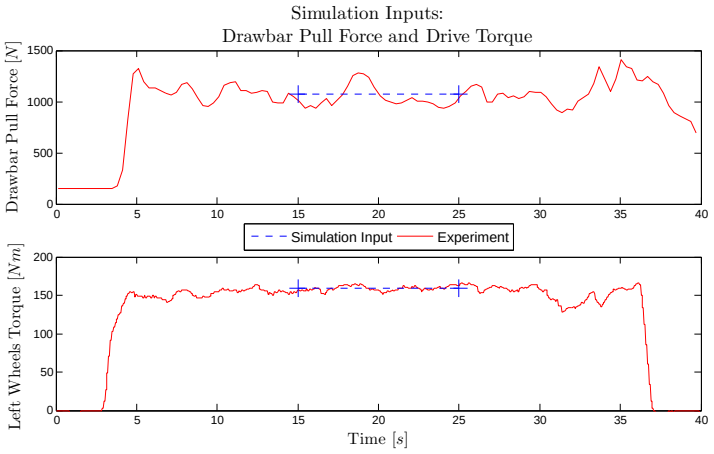

FIGURE 6. OPTIMIZATION INPUTS FROM EXPERIMENTAL DATA OF THE 2ND DRAWBAR PULL TEST

Figure 7 shows the measured longitudinal velocity and wheel spin that define the optimization objectives. In this iteration, the rover seems to be moving steadily over a time period of approximately 10s (starting at 15s). Hence, the average values of the measurements over this time period are considered for the simulation and the optimization procedure.

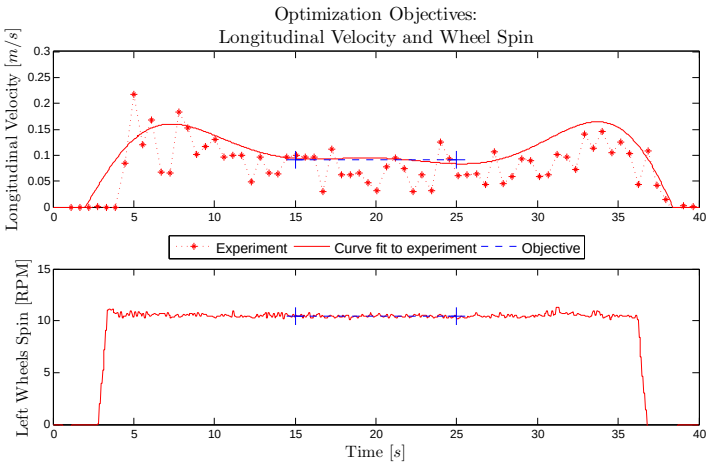

FIGURE 7. OPTIMIZATION OBJECTIVES FROM EXPERIMENTAL DATA OF THE 2ND DRAWBAR PULL TEST

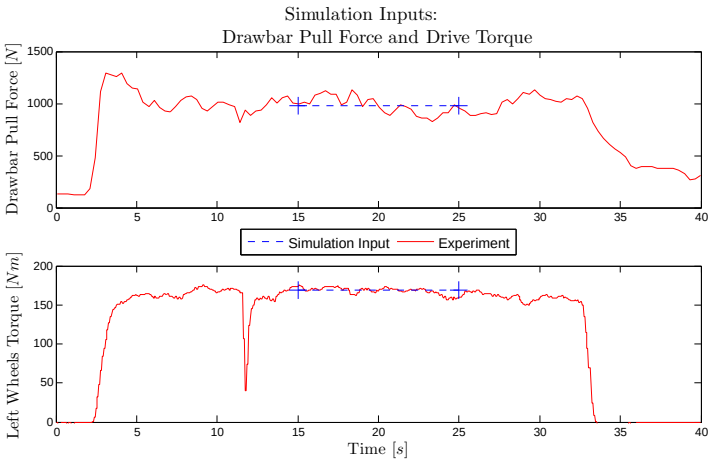

FIGURE 8. OPTIMIZATION INPUTS FROM EXPERIMENTAL DATA OF THE 3RD DRAWBAR PULL TEST

Using the same initial parameters as in the previous experiment and the averaged values for the simulation inputs and optimization objectives shown in Figure 6 and 7 respectively, this parameter identification routine settled to the values that can be observed in Table 2.

TABLE 2. WHEEL AND SOIL MODEL PARAMETERS FOR 2ND DRAWBAR PULL EXPERIMENT

Model Parameter	Initial Value	Final Value
Foundation Stiffness k_h $[N/m^{2+\eta}]$	$2.5E10^5$	$1.58E10^5$
Nonlinearity Exponent η	0.5	0.501
Foundation Rebound γ [%]	0.15	0.0813
Traction Modulus K_{v_x}	0.5	0.819

Third Drawbar Pull Experiment This third and last run of the drawbar pull test was performed over a period of approximately $32s$. The measured drawbar pull force and drive torque of this experiment that are applied to the rover model can be seen in Figure 8.

The measured longitudinal velocity and wheel spin that define the optimization objectives are illustrated in Figure 9. For this experiment, the time period of $10s$ (starting at $15s$) is considered to determine the average values of the simulation inputs and the optimization objectives.

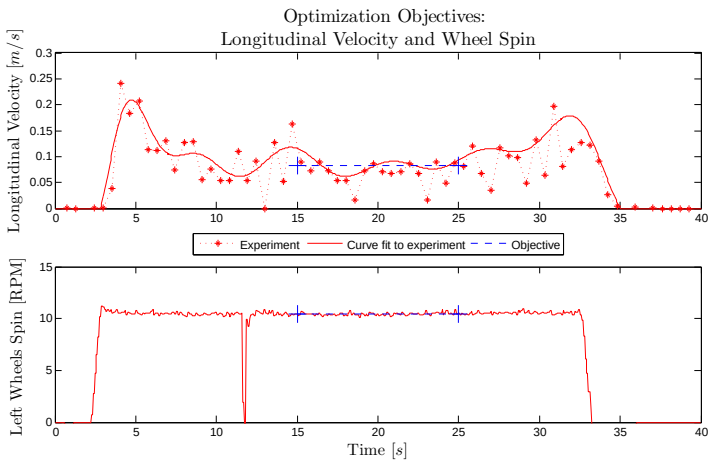

FIGURE 9. OPTIMIZATION OBJECTIVES FROM EXPERIMENTAL DATA OF THE 3RD DRAWBAR PULL TEST

Again, the optimization routine is initialized with the same values of the model parameters and the unconstrained parameters identification routine reaches the final values listed in Table 3.

TABLE 3. WHEEL AND SOIL MODEL PARAMETERS FOR 3RD DRAWBAR PULL EXPERIMENT

Model Parameter	Initial Value	Final Value
Foundation Stiffness k $[N/m^{2+\eta}]$	$2.5E10^5$	$1.47E10^5$
Nonlinearity Exponent η	0.5	0.533
Foundation Rebound γ [%]	0.15	0.0834
Traction Modulus K_{v_x}	0.5	0.794

The previous sections have shown that the three different experiments and the corresponding parameter identification routines lead to varying sets of model parameters, albeit very similar ones. Each of these parameter sets define a slightly different planetary rover wheel model given by Eqns and . These models with the individual sets of parameters are then considered to find the best curve fit to the data points taken from the experiments. The traction force ratio of the resulting wheel model is plotted over the longitudinal slip ratio and can be seen in Figure 10.

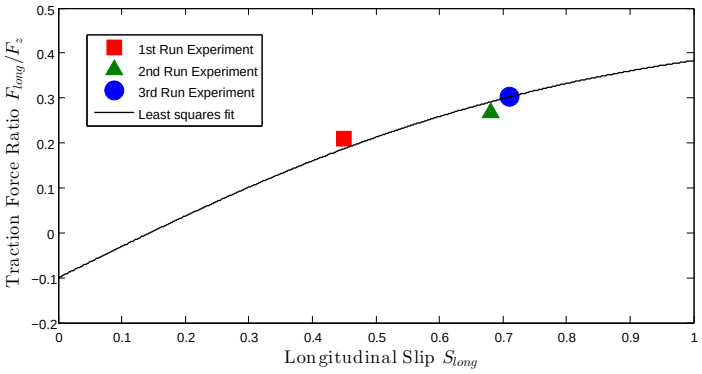

FIGURE 10. COMPARISON OF THE IDENTIFIED MODEL PARAMETERS

The curve in the plot of Figure 10 shows the characteristic behaviour of the developed planetary rover wheel model. To further validate the proposed modelling approach, the tire model with the identified parameters is simulated in a rover manoeuvre on an irregular 3-dimensional terrain and compared against experimental results. For that purpose, the parameters identified using the 2nd data set are used in the following simulations. Due to the fact that the measurements of the kinematic data show the best steady state conditions, this data set is assumed to be the most trustworthy.

VALIDATION VIA DYNAMIC SIMULATION ON 3D TERRAIN

To verify the parameters and validate the planetary rover wheel model, an experiment is performed in which the rover is commanded to move over uneven terrain. The results of this experiment are compared against the simulation results from the Juno rover model on a 3-dimensional terrain. The experiment and the comparison of the results with the simulation outcome are discussed in the following section.

LIDAR scan data from the irregular terrain is added to the MapleSim implementation of the CSA Juno rover model shown in Figure 3. The terrain data is used as an additional input to the volumetric rover wheel model and a forward dynamics simulation using the found wheel/soil interaction model parameters is run.

Irregular Terrain Experiments

For the 3-dimensional terrain experiment, the rover was operated on irregular uncompacted soft soil. An appropriate area of roughly 20 m^2 was prepared. The experiment was performed by applying a constant throttle setting of 45 % to the DC motors of the rover and by letting the rover drive freely over an irregular terrain including a mound of approximately $0.5m$ in height. The following list summarizes the crucial measurements that were taken during this experiment and the equipment needed:

Rover IMU — chassis accelerations and angular rates
Motor — current measurement (left and right side)
Motor encoder — angular speed (left and right side)
Total station — rover position (through prism attached to rover chassis)
LIDAR scanner — irregular terrain surface scan

It should be noted that apart from the measurement equipment on the rover and the total station, the terrain was scanned before the vehicle manoeuvring using a LIDAR system. The irregularly scattered LIDAR scan data is used to create a numerical representation of the uneven terrain that can be used in the simulation of the Juno rover. Therefore, raw data is cut down and transformed into an elevation function of the horizontal x and y-coordinates. A surface plot of this elevation function representing the 3-dimensional terrain is shown in Figure 11.

The presented elevation $z(x,y)$ and the surface normal function $\mathbf{n}_S(x,y)$ that returns a unit vector of the surface normal direction are implemented into the rover wheel model in MapleSim to extend this model with 3-dimensional terrain capabilities. Knowing the surface normal $\mathbf{n}_S$, the tangential directions are determined based on the orientation of the wheel hub frame. With the assumption of a locally flat terrain, the local contact problem is calculated using the hypervolume model as previously explained. All resulting forces and moments are transformed into the wheel hub frame and applied accordingly. To compare the

virtual results against the experimentally obtained data, the rover is simulated in a forward dynamics simulation using a simple PID controller on motor torques to force the rover to follow the measured wheel spins. The results of this simulation are presented below as a final step of this validation process.

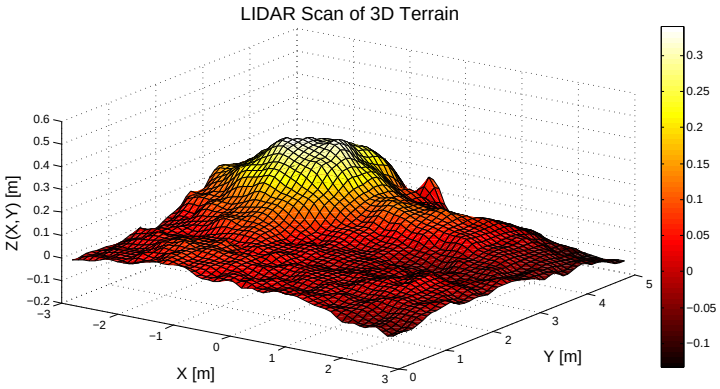

FIGURE 11. SCANNED 3D TERRAIN OF EXPERIMENT

Irregular Terrain Simulation

It should be noted that the simulated rover has to go through a settling phase. As a result, the virtual rover starts with an initial velocity unlike the actual rover that starts from rest. This is the reason for the initial difference in the plots. Figures 12 to 14 show the results of the simulation directly compared against the measurements taken during the 3-dimensional terrain experiment. The results of the longitudinal dynamics can be seen in the position and velocity plot of Figure 12.

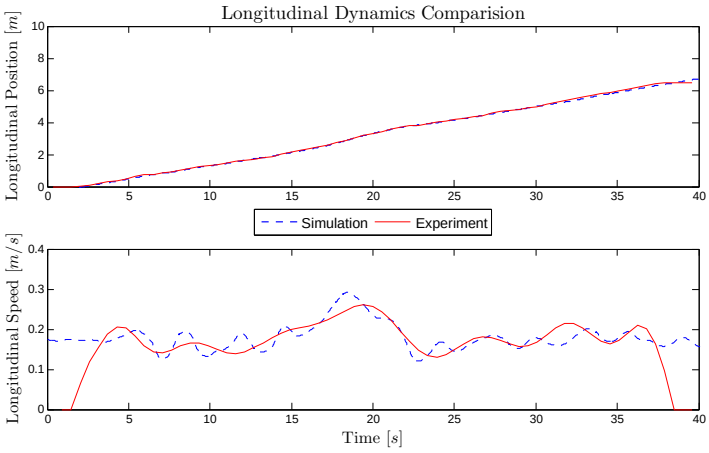

FIGURE 12. COMPARISON OF LONGITUDINAL DYNAMICS

The velocity plot shows the performance of the PID controller and it reveals that the forward velocity of the simulated rover fluctuates around the measured longitudinal speed. However, the overall performance appears to be reasonable which can be seen in the position plot of Figure 12.

The results of the right and left side wheel spin can be seen in Figure 13.

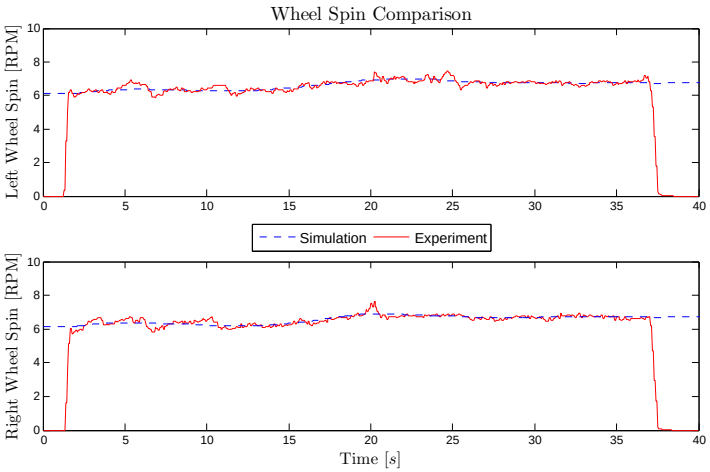

FIGURE 13. COMPARISON OF WHEEL SPIN

It can be seen in both plots of Figure 13 that the angular spin of the right and left side wheels match the experiments within a reasonable range. This means that the rover undergoes similar slip conditions during the span of the experiment.

Finally, the results of the right and left drive torques as applied to the right and left set of wheels are illustrated in Figure 14.

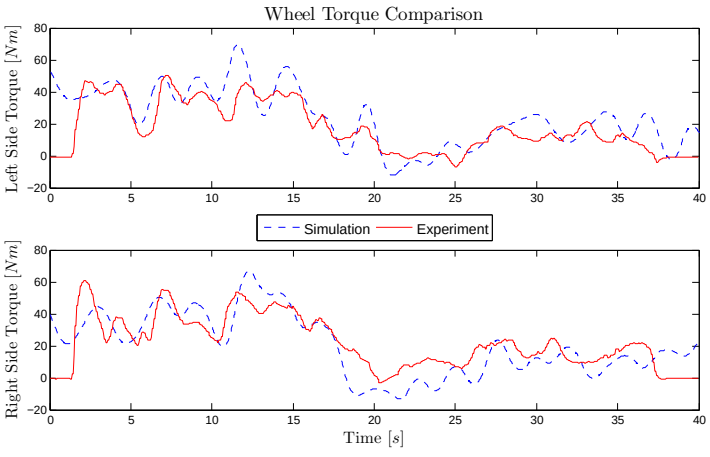

FIGURE 14. COMPARISON OF DRIVE TORQUES

In the plots of the drive torques, the total of the two wheel torques of each side is shown as it was supplied by the DC motors. It can be observed that the torques mostly agree with the experiments. The differences between the measured and the simulated drive torques can be related to a few error sources. The main reason is certainly the fact that the actual soil properties vary over the span of the terrain, whereas the assumption of homogeneous soil properties was utilized in the presented wheel/soil interaction model. Also, due to limited accuracy of the LIDAR system, there are slight differences between the actual and the numerically implemented terrain, which means that especially local bumps in the terrain may not be perfectly aligned with the simulated version. Finally, due to the performance of the PID controller, the torque fluctuates around the desired torque as seen in the longitudinal velocity plot. That being said, both plots in Figure 14 show a similar characteristic torque profile, which validates the volumetric planetary rover wheel with the identified soil foundation parameters.

CONCLUSION

A novel wheel/soil contact model based on the properties of the hypervolume of penetration is presented. In addition to the nonlinearity of the soil foundation, the developed interaction model is also capable of representing the plasticity of the soil in the form of soil rebound. Besides the geometry and inertia parameters of the contact model, four soil parameters $\mathbf{a} = [k_h, \eta, \gamma, K_{v_x}]$ that are difficult to measure remain to be identified. These parameters were found through a parameter identification process based on the Nelder-Mead algorithm by comparing the simulation results against experimental data obtained from a drawbar pull test of the Juno rover. As a final step, the developed model was extended to simulate rover motion over 3-dimensional terrains. The results of a simulation on irregular terrain using the found soil parameters compare favourably against experimental results from the CSA Juno rover. In conclusion, the developed hypervolume model with the identified parameters is adequately confirmed by the experiments through this two-step validation process.

ACKNOWLEDGMENT

The authors gratefully acknowledge the financial support of this research by the Canadian Space Agency and the Natural Sciences and Engineering Research Council of Canada. The authors would also like to thank Neptec Design Group Ltd. for the support with the experiments.

REFERENCES

[1] Wong, J., 1967. "Behaviour of soil beneath rigid wheels". *Journal of Agricultural Engineering Research,* ***12***(4), pp. 257–269.

[2] Wong, J., 2010. *Terramechanics and Off-Road Vehicle Engineering — Terrain Behaviour, Off-Road Vehicle Performance and Design*, 3rd ed. Elsevier Ltd.

[3] Ishigami, G., Miwa, A., Nagatani, K., and Yoshida, K., 2007. "Terramechanics-based model for steering maneuver of planetary exploration rovers on loose soil". *Journal of Field Robotics,* ***24***(3), pp. 233–250.

[4] Scharringhausen, M., Beermann, D., Krömer, O., and Richter, L., 2009. "A wheel-soil interaction model for planetary application". In 11th European Regional Conference of ISTVS, Bremen.

[5] Favaedi, Y., Pechev, A., Scharringhausen, M., and Richter, L., 2011. "Prediction of tractive response for flexible wheels with application to planetary rovers". *Journal of Terramechanics,* ***48***, pp. 199 – 213.

[6] Iagnemma, K., Senatore, C., Trease, B., Arvidson, R., Bennett, K., Shaw, A., Zhou, F., Van Dyke, L., and Lindemann, R., 2011. "Terramechanics modeling of mars surface exploration rovers for simulation and parameter estimation". In ASME International Design Engineering Technical Conference & Computers and Information Engineering Conference IDETC/CIE 2011.

[7] Trease, B., Arvidson, R., Lindemann, R., Bennett, K., Zhou, F., Iagnemma, K., Senatore, C., and Van Dyke, L., 2011. "Dynamic modeling and soil mechanics for path planning of mars exploration rovers". In ASME International Design Engineering Technical Conference & Computers and Information Engineering Conference IDETC/CIE 2011.

[8] Petersen, W., and McPhee, J., 2013. "A nonlinear volumetric contact model for planetary rover wheel/soil interaction". In ASME International Design Engineering Technical Conferences & International Conference on Multibody Systems, Nonlinear Dynamics, and Control.

[9] Petersen, W., 2012. "A volumetric contact model for planetary rover wheel/soil interaction". Phd dissertation, Department of Systems Design Engineering, University of Waterloo, Canada.

[10] Petersen, W., and McPhee, J., 2012. "Identification of volumetric wheel/soil interaction model parameters from planetary rover experiments". In 12th European Conference on Terrain-Vehicle Systems ISTVS, Pretoria, South Africa.

[11] Senatore, C., and Iagnemma, K. D., 2011. "Direct shear behaviour of dry, granular soils for low normal stress with application to lightweight robotic vehicle modelling". In 17th International Conference on Terrain-Vehicle Systems ISTVS, Blacksburg, Virginia, USA.

[12] Scharringhausen, M., Beermann, D., Krömer, O., and Richter, L., 2009. "Single-wheel tests for planetary applications at dlr bremen". In 11th European Regional Conference of ISTVS, Bremen.